Available online at www.sciencedirect.com
SCIENCE DIRECT
Polymer 47 (2006) 1101–1107
polymer
www.elsevier.com/locate/polymer

Transitions of domain ordering and domain size in a spherical-forming polystyrene-*block*-poly(ethylene oxide) copolymer and its composites with colloidal cadmium sulfide quantum dots

Ya-Sen Sun [a], U-Ser Jeng [a,*], Keng S. Liang [a], Siao-Wei Yeh [b], Kung-Hwa Wei [b]

[a] *National Synchrotron Radiation Research Center, 101 Hsin-Ann Road, Science Industrial Park, Hsinchu 30076, Taiwan, ROC*
[b] *Department of materials Science and Engineering, National Chiao Tung University, Hsinchu 30049, Taiwan, ROC*

Received 10 June 2005; received in revised form 4 November 2005; accepted 11 December 2005

Abstract

With specific annealing schemes applied to a neat polystyrene-*block*-poly(ethylene oxide) (SE) and its composites with cadmium sulfide quantum dots (CdS QD), we have observed microdomain structures and phase transitions in the system using temperature-resolved small-angle X-ray scattering (SAXS) and transmission electron microscopy (TEM). Both TEM images and SAXS results show clearly that incorporation of surfactant-tethered CdS QD preferentially into PEO blocks leads to increases in thermal stabilities of both bcc-packed lattice (referred as long-range order) and microdomains themselves in the sphere-forming SE/CdS composites. The bcc-packed lattice in the SE/CdS composites sustains better than that in the neat SE, during a temperature elevation to ~160 °C, at which the bcc-packed SE/CdS spheres start to transform into micelles with a short-range liquid-like order. Quantitative model analysis shows that the PEO/CdS micelles can retain their size in the SE/CdS composites up to 200 °C, whereas the PEO micelles shrink after the softening of the PS matrix around 100 °C, and disassociate largely into the PS matrix of the neat SE at 160 °C.

Keywords: Copolymer-nanoparticle composite; Microdomain; Phase transition

1. Introduction

Mixtures of solid nanoparticles and block copolymers have received considerable attention because the incorporation of nanoparticles into block copolymers produces novel and unique electronic, optical and magnetic properties [1–7]. Achieving such novel properties generally requires the fabrication of both nanoparticles and block copolymers in a nanometer scale. Copolymer–nanoparticle composites possess various complicated morphologies that offer diverse and versatile benefits, such as templates for lithography [8–10] and fabrication of metallized nanowire/nanodots [11–13]. Nevertheless, the addition of nanoparticles into block copolymers entangles the ordering phase of the neat block copolymers, due to additional interactions between the particles and copolymers.

Effects of nanoparticles on the morphological structure of copolymer–nanoparticle composites have been widely explored [14–21]. Basing on theoretical models, Balazs and coworkers predicted that copolymer–nanoparticle composites possess rich morphologies [14–17]; they concluded that interactive particles added into block copolymers are not passive but can affect significantly the overall morphology of the composite in both the strong and intermediate segregation limits of the diblock melt [17]. Experimentally, Yeh et al. found that morphological modification was induced upon incorporation of surfactant-modified CdS, of a preferential binding to the minor PEO block, into a SE copolymer [18]. Many theoretical predictions and experimental observations for ordered morphologies of copolymer–nanoparticle composites focus on the strong and intermediate segregation limits of the diblock melt [14–19]. Yet, much remains unknown about plausible transitions upon annealing copolymer–nanoparticle composites to high temperatures.

Very recently, we have reported phenomenologically the enhanced thermal stability of nanoparticle/copolymer composites over the neat copolymer, due to the formation of PEO/CdS microdomains [21]. In this contribution, we focus on the form

* Corresponding author. Tel.: +886 3 578 0281x7108; fax: +886 3 578 3813.
E-mail address: usjeng@nsrrc.org.tw (U.-S. Jeng).

0032-3861/$ - see front matter © 2005 Elsevier Ltd. All rights reserved.
doi:10.1016/j.polymer.2005.12.055

factor evolution of the microdomains of PEO/CdS and PEO in the composites and neat copolymer, respectively, during a heating process from an ordered phase to a disordered structure. The evolutions of the form factor of the microdomains and domain ordering are closely traced by temperature-resolved SAXS measurements. With a model analysis that takes into account the polydispersity of the scattering form factor $P(q)$ of the microdomains, we compare quantitatively the order–disorder transitional behaviors of the PEO/CdS and pure PEO microdomains during the heating process.

2. Experiments

2.1. Material and sample preparation

An asymmetric SE diblock copolymer with a molar-mass ratio 125 K/16.1 K was purchased from Polymersource Inc., with a volume fraction of the minor PEO block 0.11 ($f^{v}_{PEO} = 0.11$), and a polydispersity (PDI) 1.04. CdS quantum dots (QD), characterized previously with a mean size of 3.8 nm and a polydispersity of ~50%, were synthesized with mercaptoethanol as surfactant on reacting cadmium acetate dihydrate ($Cd(Ac)_2 \cdot 2H_2O$), sodium sulfide (Na_2S) and mercaptoethanol (HSC_2H_4OH) in methanol, according to a modification of the kinetics-trapping method [22,23]. After filtration, CdS QD were collected and then dissolved in *N*,*N*-dimethylformamide (DMF). The non-aggregate distribution of the CdS QD in both solutions and bulk samples were described in our previous papers [18,21].

CdS QD solutions of two concentrations, 1.8% v/v (CdS(1)) and 7.2% v/v (CdS(4)) with respect to the PEO block, were added, respectively, into the SE/DMF solutions under stirring. Two composites, designated as SE/CdS(1) and SE/CdS(4) depending on unsaturated and saturated CdS concentrations incorporated into SE copolymers, were cast from the DMF solutions. To avoid crystallization-induced metastable phases in the solution-cast SE and its composites, bulky specimens were cast from the DMF solutions and then annealed under DMF vapor at 60 °C for 12 h. After the development of thermal equilibrium with microphase-separated microdomains, residual solvent was further removed under vacuum at 60 °C for 1 week.

2.2. Apparatus

SAXS experiments were performed at the wiggler beamline BL17B1 at the National Synchrotron Radiation Research Center (NSRRC), Taiwan, with a monochrome beam of a wavelength of $\lambda = 1.6$ Å. The distance from sample to detector was 975 mm and the beam stop was a molybdenum disk of a diameter 4 mm. SAXS data were collected using a one-dimensional position-sensitive detector, calibrated with a Fe^{55} source before the data collection. All the SAXS data were corrected, respectively, for sample transmission, background and detector sensitivity, and normalized to the absolute scattering scale $I(q)$, namely, the differential scattering cross section $d\sigma/d\Omega$ per unit sample volume. The absolute scattering

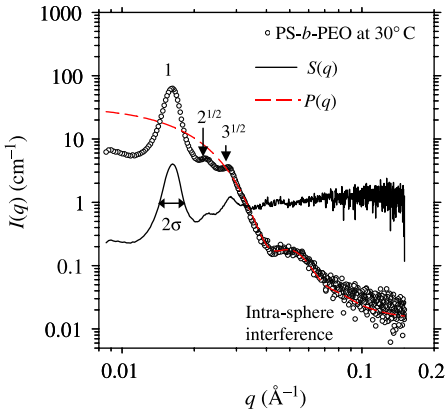

Fig. 1. SAXS data for the neat SE as cast from the DMF solution and the corresponding curve-fitted patterns for structure factor, $S(q)$ and form factor, $P(q)$.

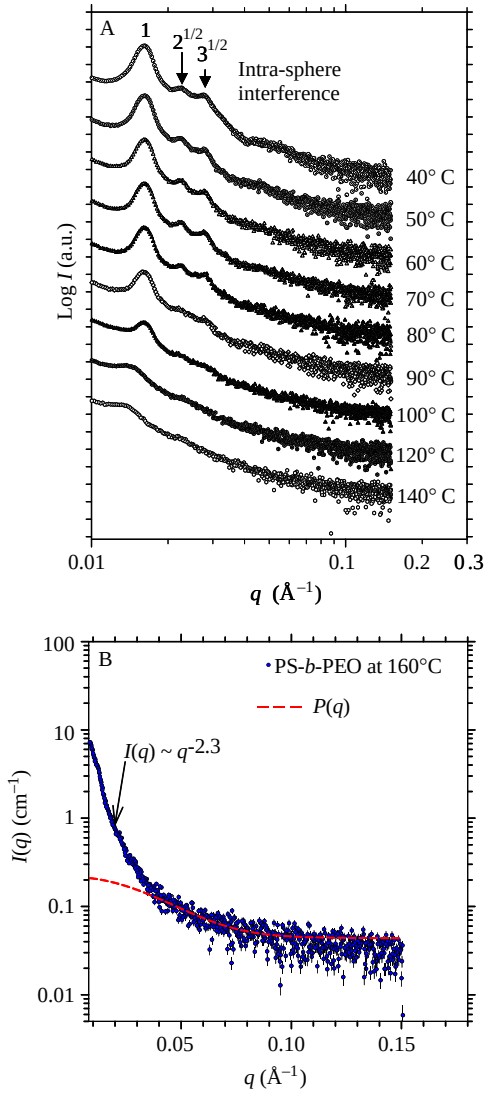

Fig. 2. (A) Temperature-dependent SAXS profiles for the neat SE block copolymer subjected to heating in the temperature range 40–140 °C. (B) SAXS data (solid circles) and the corresponding curve-fitting pattern (short dotted curve) for the neat SE annealed at 160 °C.

Table 1
Structural parameters for the SE, SE/CdS(1), and SE/CdS(4) samples

	T (°C)	d (nm)	p	D (nm)	L (nm)	Nor. Q_{inv}
SE	30	20.8	0.15	47.6	350	1
	100	13.8	0.33	Lattice disorder		0.41
	160	7.0	0.4	Melt/disorder micelles		0.4
SE/CdS(1)	30	21.4	0.15	67.0	224	1
	200[a]	27.0	0.26	Disorder micelles		0.55
SE/CdS(4)	30	27.4	0.2	69.8	332	1
	200[a]	28.0	0.26	Disorder micelles		1

The normalized Q_{inv} is the normalized scattering power with respect to the Q_{inv} value at 30 °C.
[a] The data of the composites at 200 °C are adopted from our previous study [21].

intensity is critical in calculating the scattering invariant Q_{inv} for assessing quantitatively the degree of phase separation in the system [21]. The scattering wavevector transfer q is defined as $q=(4\pi/\lambda)\sin(\theta/2)$ in which θ is the scattering angle. The specimens were placed in a sample cell sealed with two thin Kapton films, and heated to designated temperatures under a nitrogen environment for SAXS measurements. For each set of 10-min. SAXS data collection, 15 min. were awaited for thermal equilibrium after the sample reached the target temperature.

TEM experiments (Hitachi H-600) were performed with an accelerating voltage 120 kV. Thin slices were prepared using a microtome (Leica Ultracut Uct) on the diblock copolymer and composites. To increase the phase contrast of microdomains, we stained the neat SE diblock copolymer under RuO_4 vapor at 25 °C for 12 h. The stain was not necessary for the composites due to the high electron density of CdS QD. TEM images were taken for the as-cast SE/CdS composites and the composites annealed at 140 and 200 °C for 12 h, then followed by rapid quenching in liquid nitrogen.

3. Results and discussion

Fig. 1 shows the SAXS pattern (open circles) for the as-cast SE copolymer measured at 30 °C, featuring with the relatively sharp diffraction peaks located at $q=0.0162$, 0.0225 and 0.0280 $Å^{-1}$, respectively. These peaks with the q ratios of $1:2^{1/2}:3^{1/2}$ are the characteristic diffractions of spherical domains, ordering with a body-cubic-center (bcc)-packed lattice. On the other hand, a broad scattering hump at q near 0.05 $Å^{-1}$ reflects the form factor scattering of individual spherical domain [24]. Using a model of polydisperse spheres, with a mean radius of 10.4 nm and a polydispersity of 15% (dashed curve), we can reproduce the form factor scattering $P(q)$ in the q region from intermediate to large q (Fig. 1), where the structure factor $S(q)$ has a much less influence. The interference $S(q)$ is, then, extracted from $I(q)/P(q)$ [19,21]. An inter-domain spacing $D=47.6$ nm can be estimated from the position of the principal peak, whereas the size of the long-range-order domain $L\sim350$ nm can be extracted from the half-height-full-width 2σ of the principal peak, using $L\propto\pi/\sigma$.

For the as-cast SE copolymer, the impact of the crystallization of PEO blocks on the morphology of the SE copolymer is suppressed upon casting at 60 °C, a temperature above the melting temperature of PEO (~45 °C). Thus, the morphology of spherical microdomains with the bcc-packed lattice in the neat SE is mainly driven by microphase separation. Note, with the intervening of the crystallization kinetics of PEO blocks upon casting the SE at 25 °C, a metastable phase of cylinder-like domains in a hexagonal array was obtained in our previous report [18].

Fig. 2 shows the temperature-resolved SAXS profiles for the neat SE subjected to successive heating in a temperature range 40–140 °C. Before softening of the PS matrix (~98 °C), the structural factor $S(q)$ maintains relatively stable in the temperatures of 40–80 °C. Nevertheless, the total scattering intensity decreases quickly as temperature increases and approaches the melting temperature of PEO (~45 °C), due to the smaller contrast between the PS matrix and the amorphous PEO domains. Starting from 90 °C, the PS matrix softens. The depressed and broadened ordering peaks indicate an occurrence of lattice disordering. Upon heating to 120 and 140 °C, $S(q)$ for the pure PEO domains is largely diminished, and the SAXS patterns show a nearly monotonic scattering with little discernible characteristics of diffraction peaks. Upon further heating the SE sample at 160 °C, a SAXS pattern shows a diffuse scattering with absence of characteristic diffraction

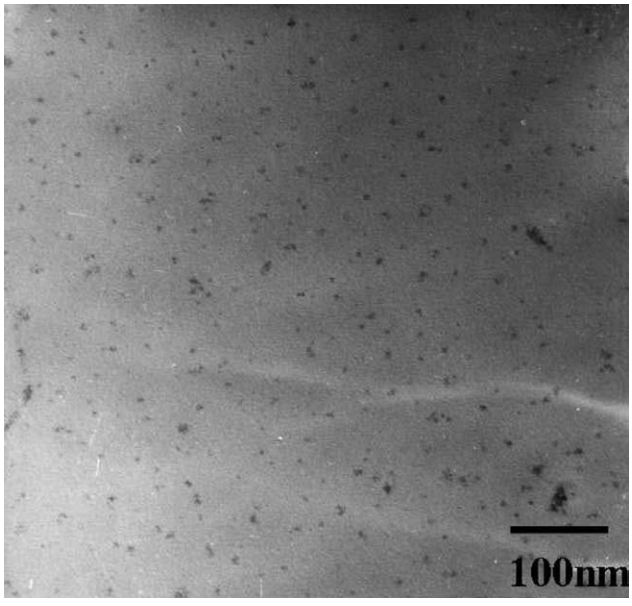

Fig. 3. TEM image of the SE block copolymer after isothermal annealing at 140 °C followed by rapid quenching in liquid nitrogen.

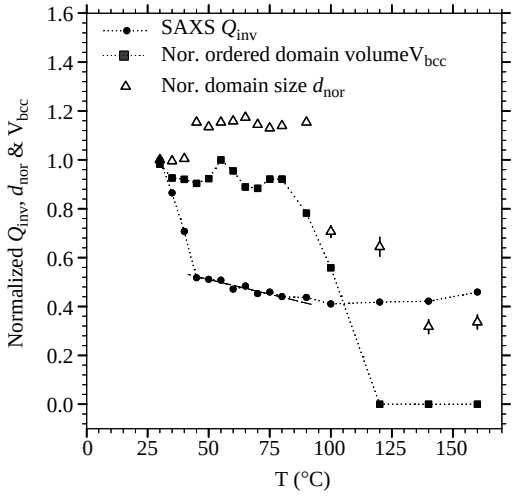

Fig. 4. Normalized Q_{inv}, d_{nor}, and ordered phase volume V_{bcc} as a function of temperature for the neat SE block copolymer.

peaks, as shown in Fig. 2(B), where the data in the q region from intermediate to high q can be fitted with a model of spherical domains of a mean radius of 3.5 nm and a polydispersity of 40%. On the other hand, the data in the low-q region can be characterized by $I(q)$–$q^{-2.3}$, revealing a sign of thermal composition fluctuations. This result indicates that upon annealing at 160 °C the PEO micellar size becomes small. When the micellar size is smaller than a critical size for achieving stable microphase-separated domains, the PEO micelles dissociate largely into the PS matrix. Similar phenomena have been found in highly asymmetric polystyrene-*block*-polyisoprene and polystyrene-*block*-polyisoprene-*block*-polystyrene copolymers [25,26]. The structural parameters extracted for the PEO domains at each temperature using the same model stated previously are tabulated in Table 1.

Fig. 3 reveals a TEM image for a thin section of this neat SE sample after having been subjected to extended annealing at 140 °C for 12 h followed by rapid quenching in liquid nitrogen.

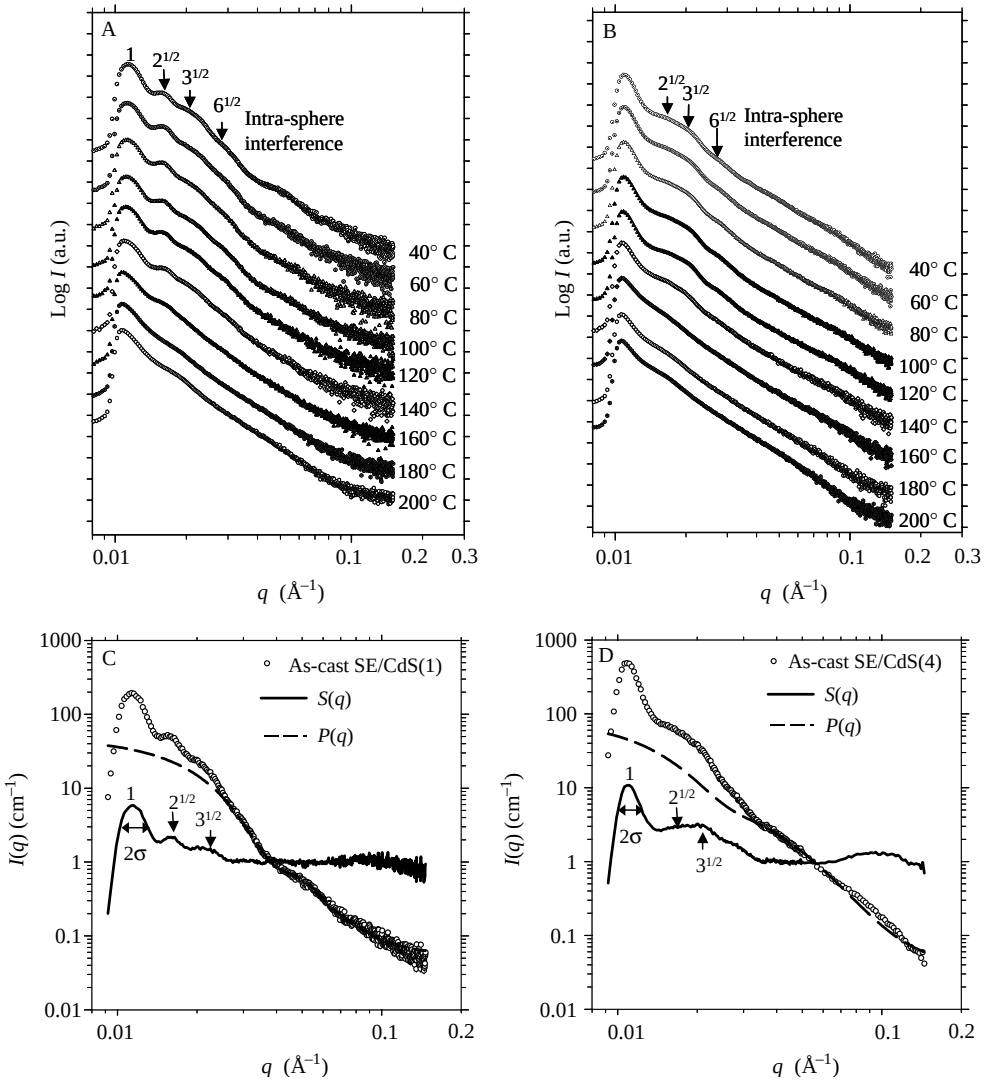

Fig. 5. Temperature-dependent SAXS profiles for (A) SE/CdS(1) and (B) SE/CdS(4) composites. The curves in (C) and (D) show, respectively the SAXS data and the corresponding simulations for the as-cast composites.

The TEM image clearly shows small micelles (~8 nm in diameter) randomly dispersed in the PS matrix.

For clearly identifying the morphological change as a function of annealing temperature, the temperature dependence of the normalized invariant $Q_{inv}(T)/Q_{inv}(T_0)$ and volume $V_{bcc}(T)/V_{bcc}(T_0)$ of the long-range-order domains are shown in Fig. 4, where T_0 is a reference temperature. Here we use Q_{inv} (30 °C) and V_{bcc} (30 °C) for the as-cast SE at 30 °C as the reference quantities. From 30 to 80 °C, V_{bcc} persists well, indicating that the bcc-packed order maintains well in the solid PS matrix. On the other hand, the ~65% drop in Q_{inv} in this temperature range can be quantitatively explained by the reduced electron contrast due to the smaller density differences between PEO and PS blocks for the SE at 80 °C [27]. In the temperature range 80–100 °C (approaching the glass-transition temperature (T_g^{PS}) of the PS matrix and order–disorder transition temperature (T_{ODT}) of the neat SE), V_{bcc} depresses significantly as the bcc-packed spheres gradually transform into disorder micelles with a short-range liquid-like order. At temperatures above 120 °C, the disorder micelles become less stable with rising temperature and successively dissociate to homogeneous melt with thermal fluctuations, leading to a vanishing V_{bcc} value. Nevertheless, these residual PEO micelles together with the density fluctuations of the neat SE contribute to the Q_{inv} values measured above 120 °C, as shown in Fig. 4.

Fig. 5 presents temperature-resolved SAXS profiles for (A) SE/CdS(1) and (B) SE/CdS(4) composites subjected to a series of temperature increase in steps of 20 °C from 40 to 200 °C. For both the as-cast SE/CdS composites, SAXS profiles show several broad diffraction features, which are characteristics of bcc-packed spheres, as illustrated in Fig. 5(C) and (D). Using the same model of polydisperse spheres as that for the neat SE, structural parameters for the two as-cast composites, such as PEO/CdS domains size d, polydispersity p, domain spacing D, order length L and normalized Q_{inv}, are extracted and tabulated in Table 1.

Upon increase of temperature from 40 to 140 °C, these diffraction peaks retain the same positions and intensities. For the SE/CdS composites annealed at 160 °C, the intensity of the principal peak was depressed, accompanied by disappearance of the higher-order diffracted peaks. This SAXS result indicates that the long-range order was destroyed upon heating the SE composites at temperatures between 140 and 160 °C. However, disordered micelles exist in these SE/CdS composites, as a trace of a transformation from ordered bcc-packed spheres into disordered micelles. At 180–200 °C, the SAXS curves reveal the depressed intensities of the principal peaks, indicative of disordered micelles in SE/CdS composites.

Fig. 6(A)and (B) shows the temperature dependence of normalized Q_{inv} and normalized volume (V_{bcc}) of the long-range-order domains for the SE/CdS(1) and SE/CdS(4) composites. For both SE/CdS composites, a discontinuous change of the V_{bcc} can be observed when the ordered bcc-packed spheres transform into disordered micelles. Furthermore, Q_{inv} changes slightly or remains nearly constant for the SE/CdS composites annealed at temperatures ranging from 60

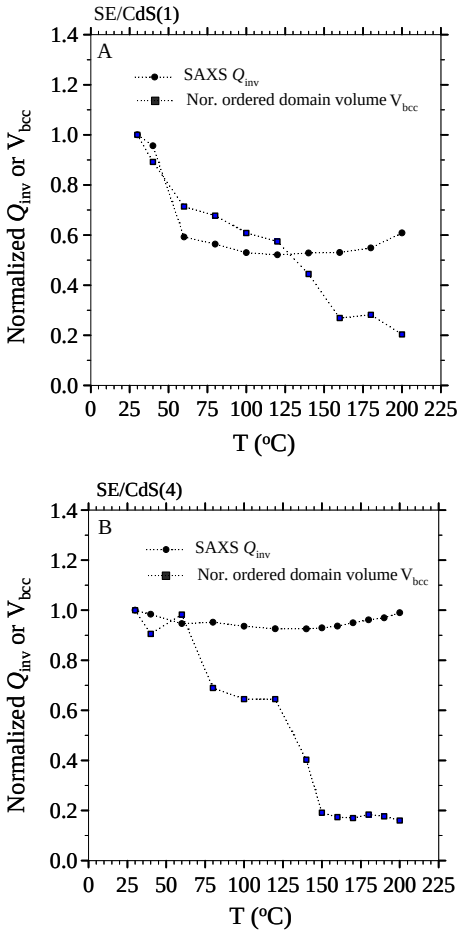

Fig. 6. Normalized Q_{inv} and ordered phase volume V_{bcc} as a function of temperature for (A) SE/CdS(1) and (B) SE/CdS(4) composites.

to 200 °C. Presumably, due to the incorporation of the CdS QD within PEO blocks, the PEO chains have to stretch to get around the dispersed nanoparticles and thus are stiffened with a reduced molecular mobility owing to the binding to the nanoparticles. Nevertheless, there is a 40% drop in Q_{inv} for the SE/CdS(1) composite in the temperature range of 30–60 °C. Since the PEO chains are not saturated with CdS QD (1.8% v/v CdS nanoparticles in the PEO domains) in the SE/CdS(1) composite, the PEO domains may crystallize when the temperatures are below the melting of the PEO crystallites [18,21]. The 40% drop in Q_{inv} for the SE/CdS(1) composite annealed in the temperature range can be explained by the reduced electron contrast due to the smaller density differences between CdS/PEO and PS blocks in the absence of the PEO crystallites. In fact, if the PEO blocks are saturated with CdS QD (for example, 7.2% v/v CdS nanoparticles in the case of SE/CdS(4) [21]), the crystallization of the PEO blocks can be completely inhibited. The SE/CdS(4) composite did not crystallize even after storage at the lowest annealed temperature of −20 °C [18]. As the PEO chains in the SE/CdS composites are comparatively less flexible (more sluggish) than those in the neat SE, the electron contrast between the PEO/CdS spheres and the PS matrix can be relatively insensitive to temperature changes. In contrast, the PEO

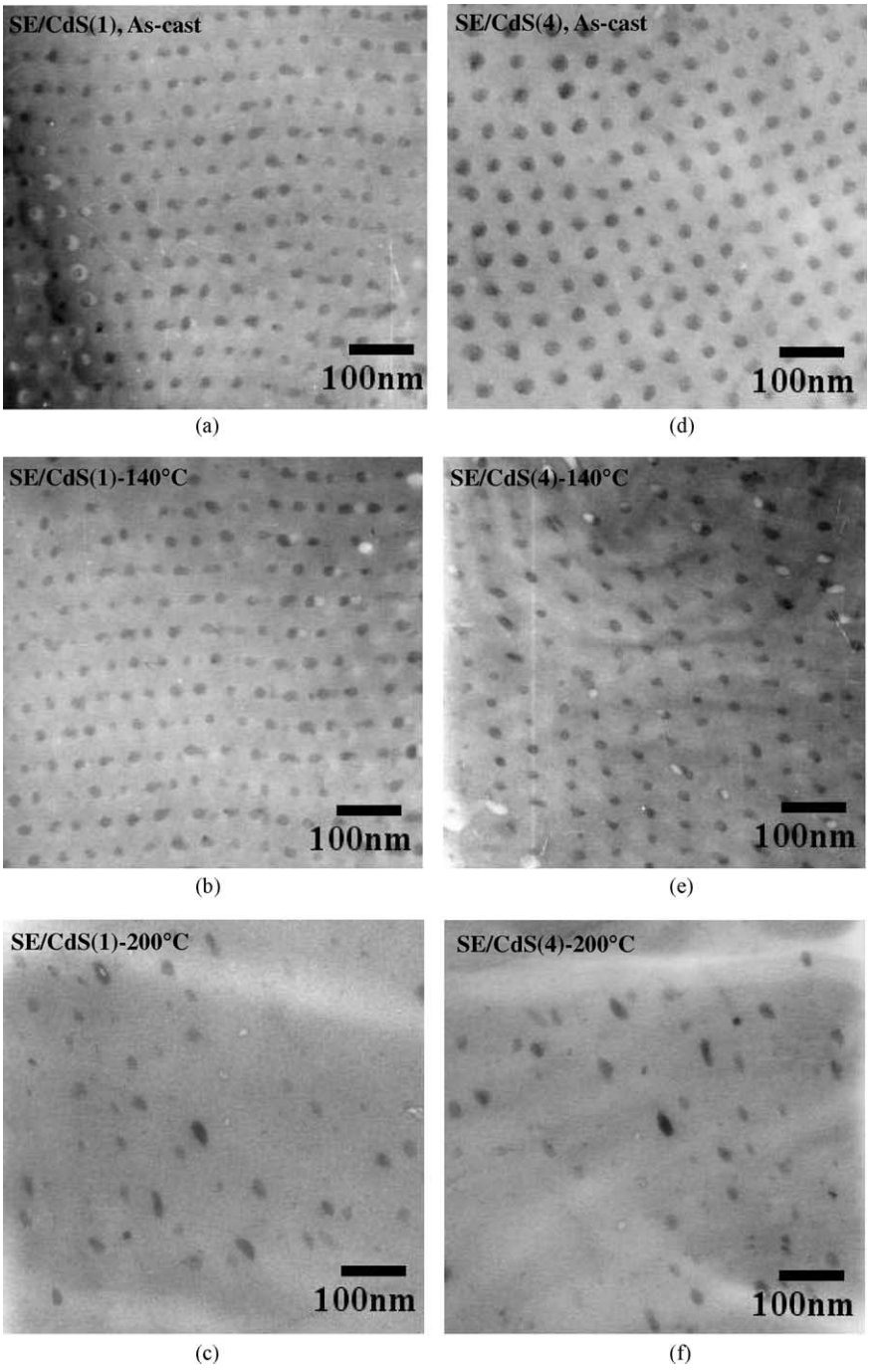

Fig. 7. TEM images of (a) SE/CdS(1) and (d) SE/CdS(4) composites taken at the as-cast form and after annealed at (b) and (e)140 and (c) and (f) 200 °C for 12 h. Image (d) is adopted from our previous paper [18].

spherical domains in the neat SE start to dissociate after softening of the PS matrix at temperatures higher than T_g^{PS} and T_{ODT} (Table 1), where T_{ODT} is close to T_g^{PS} in the case of no CdS QD particles in the SE [21].

To provide further evidence, we have employed TEM characterization to investigate the morphological evolution of the SE/CdS composites subjected to several thermal treatments. Fig. 7 presents TEM images for SE/CdS(1) and SE/CdS(4) composites. After scrutiny of these TEM images, we describe pertinent phenomena as follows. Through incorporation of surfactant-modified CdS QD into PEO blocks, the PEO block selectively stained with CdS QD appears dark, whereas PS appears white. Before further annealing, both as-cast SE/CdS(1) (Fig. 7(a)) and SE/CdS(4) (Fig. 7(d)) composites reveal bcc-packed PEO/CdS spheres in the PS matrix. At 140 °C certain spherical domains deform slightly although the bcc-packed lattice of these spheres persists largely (Fig. 7(b) and (e)). At 200 °C, disordered spheres (micelles) with a short-range liquid-like order can be observed (Fig. 7(c) and (f)).

With the SAXS evidence combined with TEM observation, we proceed to interpret the experimentally observed increase of thermal stability of bcc-packed spheres for SE composites

incorporating CdS QD in various proportions. The reason is that hydrogen bonding, between hydroxyl groups of the surfactant attached on CdS QD and ethylene oxide in the PEO domain, increases the repulsive segment–segment interaction between PS and PEO. The repulsive interaction plays a crucial role in order–disorder phase transition [28,29]. It has been proposed that the order–disorder transition temperature of microdomain structures is inversely related to this segment–segment interaction [30,31]. Thus, the order-disorder phase transition for SE/CdS composites is expected to occur at a temperature higher than that for neat SE. Furthermore, after transformation from bcc-packed spheres to disordered ones, the binding of the surfactant on the surface of CdS QD may preserve the disordered micelles of PEO/CdS from micelle dissociation into the PS matrix [21].

In summary, we have shown that the surfactant-modified CdS QD can be used to finely manipulate the thermal stability and domain sizes of microphase-separated microdomains in a diblock copolymer. In light of the spin-coated diblock copolymer–nanoparticle thin films with well-ordered microdomains being used as templates [32–34], the effective nanoparticles' binding can be extended to raise the service temperature for diblock copolymer lithography processes and control the density of periodical domains within self-assembled copolymer-based templates.

4. Conclusion

The bcc-packed PEO spheres in the neat SE block copolymer possess a relatively vulnerable thermal stability. At temperatures above 100 °C, the bcc-packed lattice of the SE is largely destroyed. And the spherical PEO domains, lacking the support from the PS matrix, disassociate gradually and transform into disorder melt largely with residual micelles of smaller size. In contrast, the incorporation of CdS QD into PEO blocks results in the same bcc-packed spherical microdomains as the neat SE, but with a greater thermal stability in the SE/CdS composites. The bcc-packed lattice of the SE/CdS composites survives up to ~160 °C. After the loss of the bcc-packed lattice, the PEO/CdS micellar domains, however, maintain their size up to the highest temperature 200 °C studied.

Acknowledgements

We thank Dr Chia-Hung Hsu, Dr Hsin-Yi Lee and Mr Chih-Mou Huang for assistance with SAXS set-up and assembly at wiggler beamline BL17B1.

References

[1] Förster S, Antonietti M. Adv Mater 1998;10:195.
[2] Simon PFW, Ulrich R, Spiess HW, Wiesner U. Chem Mater 2001;13:3464.
[3] Lopes WA, Jaeger HM. Nature 2001;414:735.
[4] Fogg DE, Radzilowski LH, Blanski R, Schrock RR, Thomas EL. Macromolecules 1997;30:417.
[5] Bockstaller M, Kolb R, Thomas EL. Adv Mater 2001;13:1783.
[6] Fink Y, Urbas AM, Bawendi MG, Joannopoulos JD, Thomas EL. J Lightwave Tech 1999;17:1963.
[7] Thurn-Albrecht T, Schotter J, Kästle GA, Emley N, Shibauchi T, Krusin-Elbaum L, et al. Science 2000;290:2126.
[8] Park M, Harrison C, Chaikin PM, Register RA, Adamson DH. Science 1997;276:1401.
[9] Park M, Chaikin PM, Register RA, Adamson D. Appl Phys Lett 2001;79:257.
[10] Cheng JY, Ross CA, Chan VZH, Thomas EL, Lammertink RGH, Vancso GJ. Adv Mater 2001;13:1174.
[11] Fahmi AW, Braun HG, Stamm M. Adv Mater 2003;15:1201.
[12] Haupt M, Miller S, Glass R, Arnold M, Sauer R, Thonke K, et al. Adv Mater 2003;15:829.
[13] Kim HC, Jia X, Stafford CM, Kim DH, McCarthy TJ, Tuominen M, et al. Adv Mater 2001;13:795.
[14] Huh J, Ginzburg VV, Balazs AC. Macromolecules 2000;33:8085.
[15] Thompson RB, Ginzburg VV, Matsen MW, Balazs AC. Science 2001;292:2469.
[16] Thompson RB, Ginzburg VV, Matsen MW, Balazs AC. Macromolecules 2002;35:1060.
[17] Lee JY, Thompson RB, Jasnow D, Balazs AC. Macromolecules 2002;35:4855.
[18] Yeh SW, Wei KH, Sun YS, Jeng U, Liang KS. Macromolecules 2003;36:7903.
[19] Yeh SW, Wei KH, Sun YS, Jeng U, Liang KS. Macromolecules 2005;38:6559.
[20] Sohn BH, Choi JM, Yoo II S, Yun SH, Zin WC, Jung JC, et al. J Am Chem Soc 2003;125:6368.
[21] Jeng U, Sun YS, Lee HY, Hsu CH, Liang KS, Yeh SW, et al. Macromolecules 2004;37:4617.
[22] Herron N, Wang Y, Eckert H. J Am Chem Soc 1990;112:1322.
[23] Veinot JGC, Ginzburg M, Pietro WJ. Chem Mater 1997;9:2117.
[24] Sakamoto N, Hashimoto T. Macromolecules 1998;31:8493.
[25] Han CD, Vaidya NY, Kim D, Shin G, Yamaguchi D, Hashimoto T. Macromolecules 2000;33:3767.
[26] Choi S, Vaidya NY, Han CD, Sota N, Hashimoto T. Macromolecules 2003;36:7707.
[27] Zhu L, Cheng SZD, Calhoun BH, Ge Q, Quirk RP, Thomas EL, et al. Polymer 2001;42:5829.
[28] Lee KM, Han CD. Macromolecules 2003;36:804.
[29] Epps III TH, Bailey TS, Pham HD, Bates FS. Chem Mater 2002;4:1706.
[30] Leibler L. Macromolecules 1980;13:1602.
[31] Hamley IW. The physics of block copolymer. New York: Oxford University Press; 1998 [chapter 2].
[32] Lin Y, Böker A, He J, Sill K, Xiang H, Abetz C, et al. Nature 2005;434:55.
[33] Yeh SW, Chang YT, Chou CH, Wei KH. Macromol Rapid Commun 2004;25:1679.
[34] Yeh SW, Wu TL, Wei KH. Nanotechnology 2005;16:683.